

Long lifetimes of quantum-dot intersublevel transitions in the terahertz range

E. A. Zibik^{1*}†, T. Grange^{2*}†, B. A. Carpenter¹, N. E. Porter¹, R. Ferreira^{2‡}, G. Bastard², D. Stehr³, S. Winnerl³, M. Helm³, H. Y. Liu^{4*}, M. S. Skolnick¹ and L. R. Wilson^{1‡}

Carrier relaxation is a key issue in determining the efficiency of semiconductor optoelectronic device operation. Devices incorporating semiconductor quantum dots have the potential to overcome many of the limitations of quantum-well-based devices because of the predicted long quantum-dot excited-state lifetimes. For example, the population inversion required for terahertz laser operation in quantum-well-based devices (quantum-cascade lasers^{1,2}) is fundamentally limited by efficient scattering between the laser levels, which form a continuum in the plane of the quantum well. In this context, semiconductor quantum dots are a highly attractive alternative for terahertz devices, because of their intrinsic discrete energy levels. Here, we present the first measurements, and theoretical description, of the intersublevel carrier relaxation in quantum dots for transition energies in the few terahertz range. Long intradot relaxation times (1.5 ns) are found for level separations of 14 meV (3.4 THz), decreasing very strongly to ~2 ps at 30 meV (7 THz), in very good agreement with our microscopic theory of the carrier relaxation process. Our studies pave the way for quantum-dot terahertz device development, providing the fundamental knowledge of carrier relaxation times required for optimum device design.

The predicted suppression of carrier relaxation rates in semiconductor quantum dots compared with quantum wells has motivated the study of quantum-dot carrier relaxation mechanisms and quantum-dot optoelectronic device development across a wide range of operating wavelengths^{3–5}. The development of efficient devices based on intraband transitions operating at mid- and far-infrared wavelengths (terahertz range), such as quantum-cascade lasers, relies on a detailed knowledge of carrier relaxation processes. Direct measurements of intersubband relaxation times in quantum wells yield times of up to 500 ps in the terahertz range, showing a strong reduction to tens of picoseconds with increasing electron density in the excited sub-band⁶. This reduction is mainly due to electron–electron scattering in the upper sub-band⁷ and heating of the two-dimensional electron gas, which permits efficient optical phonon scattering from the high-energy tail of the electron distribution⁶. In quantum dots these effects are suppressed because of the discrete nature of the energy levels. The potential for high-efficiency quantum-dot-based terahertz emitters has recently been highlighted by the record high-temperature operation of a quantum-well-based terahertz quantum-cascade laser in which extra lateral

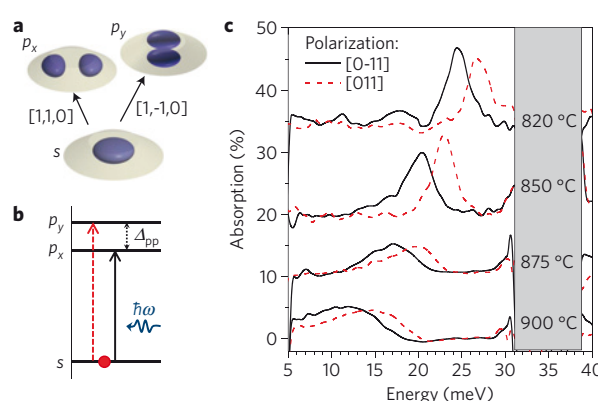


Figure 1 | Intersublevel transitions in quantum dots. **a**, Calculated wavefunctions for s-like ground and p-like first excited states in quantum dots. **b**, Schematic diagram of the energy levels of a quantum dot and allowed optical transitions. **c**, Normal-incidence absorption spectra (for two orthogonal linear light polarizations) of quantum-dot samples with different annealing temperatures measured at 10 K (the spectra are shifted for clarity).

carrier confinement was provided by high magnetic fields in the growth direction⁸.

Self-assembled quantum dots (SAQDs) are an appealing solution for device incorporation. However, carrier relaxation has been studied over only a limited range of sublevel energy separations. Typically, the transition energy between the ground and first excited conduction band states lies in the range 40–60 meV for InGaAs SAQDs, above the Reststrahlen band (36 meV ~ 9 THz). Experimental studies^{9,10} have demonstrated that the carrier relaxation in SAQDs occurs on a timescale of tens of picoseconds. This was explained in terms of anharmonicity of the polarons formed by the interaction between electrons and longitudinal optical phonons^{10–13}. However, recent theoretical work based on a microscopic approach of polaron anharmonicity¹³ has predicted a significantly longer lifetime for dots with sublevel spacing below the longitudinal optical phonon energy. Here, we report pump–probe investigations of the relaxation dynamics in InGaAs SAQDs in the few terahertz (sub-Reststrahlen) range. We show that the relaxation time shows a marked increase of three orders of magnitude over a narrow (~15 meV) energy range up

¹Department of Physics and Astronomy, University of Sheffield, Sheffield S3 7RH, UK, ²Laboratoire Pierre Aigrain, Ecole Normale Supérieure, Centre National de la Recherche Scientifique, 24 Rue Lhomond, 75005 Paris, France, ³Institute of Ion Beam Physics and Material Research, Forschungszentrum Rossendorf, PO Box 510119, 01314 Dresden, Germany, ⁴EPSRC National Centre for III–V Technologies, Sheffield S1 3JD, UK. *Present addresses: Oclaro (Switzerland) AG, Binzstrasse 17, CH-8045 Zürich, Switzerland (E.A.Z.); Walter Schottky Institut, Technische Universität München, 85748 Garching, Germany (T.G.); Department of Electronic & Electrical Engineering, University College London, London WC1E 7JE, UK (H.Y.L.). †These authors contributed equally to this work. ‡e-mail: robson.ferreira@lpa.ens.fr; Luke.Wilson@sheffield.ac.uk.

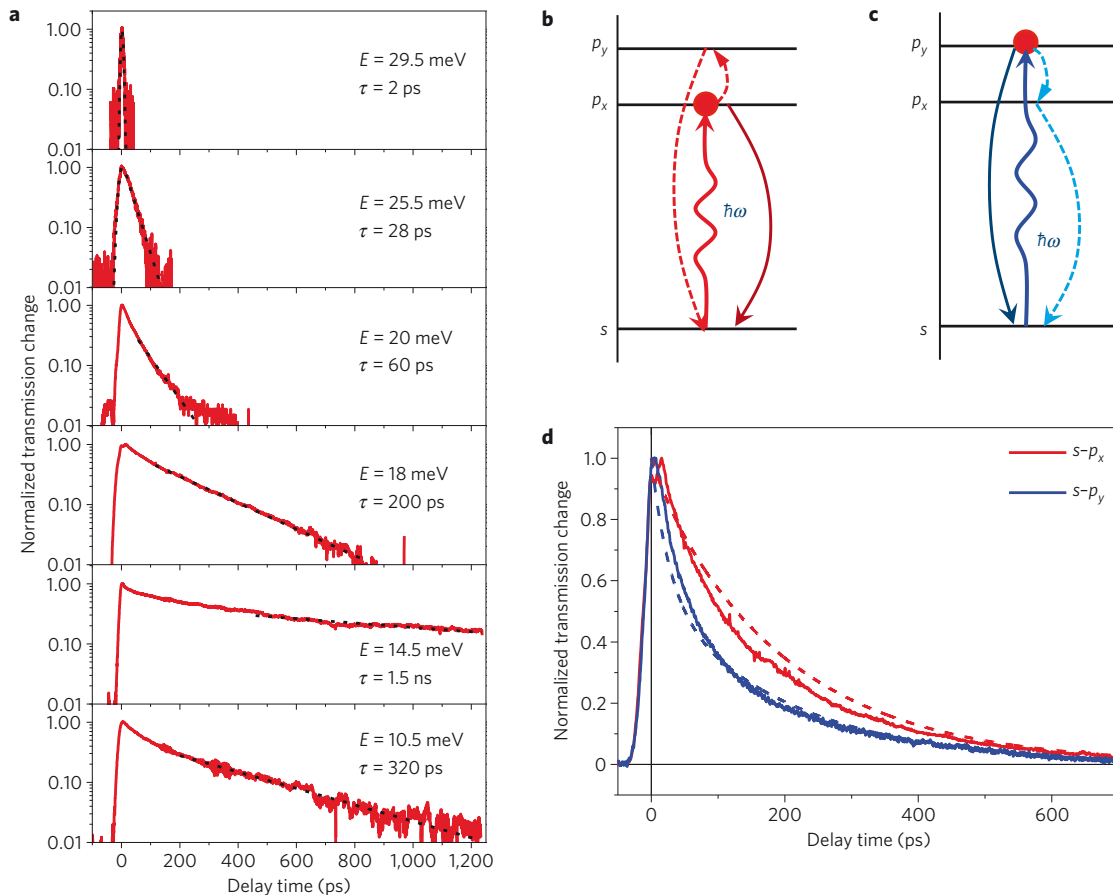


Figure 2 | Population dynamics in quantum dots. **a**, Normalized time evolution of the s - p_x intersublevel transmission change at different excitation energies at 10 K: pump-probe measurements at excitation energy E (red solid lines) and exponential fit with time constant τ (black dashed lines). **b,c**, Schematic of the possible relaxation paths after exciting either the p_x (**b**) or p_y (**c**) state. The solid arrows show the direct p -to- s intersublevel relaxation process, and the dashed arrows illustrate the relaxation path through acoustic-phonon-assisted transitions between p_x and p_y states. **d**, Pump-probe curves (solid line) for excitation into either the p_x or p_y state at the same energy of 18 meV and simulation (dashed line) taking into account the thermalization between the p states by acoustic phonon emission and absorption.

to a maximum of 1.5 ns, and we discuss model calculations that enable us to clearly identify the underlying mechanism responsible for the energy relaxation.

The investigated samples comprise 80 layers of SAQDs (areal density $\sim 4 \times 10^{10} \text{ cm}^{-2}$) separated by 50-nm-wide GaAs barriers, thus preventing both structural and electronic coupling between the layers. The dots of each layer are populated with electrons transferred from a Si-doped layer grown ~ 2 nm below them. The doping density was controlled in such a way as to charge each dot with at most one electron (see ref. 10 and references therein for more details). The fundamental intersublevel transitions occur in the mid-infrared region (around 50 meV) and involve one ground (s) state and a doublet (p_x and p_y) of excited levels (Fig. 1a). The absorption spectrum shows two inhomogeneously broadened peaks shifted by a small anisotropic splitting $\Delta_{pp} \sim 3.5$ meV, with each transition related to light polarized along either the $[1, 1, 0]$ (s -to- p_x transition) or $[1, -1, 0]$ (s -to- p_y transition) crystallographic direction (different effects have been invoked to explain the splitting of the p_x and p_y states: in-plane shape anisotropy¹⁴, piezoelectric field effects¹⁵ and atomistic symmetry¹⁶). To decrease the transition energy below the longitudinal optical phonon energy $\hbar\omega_{LO}$, we used the well-established method of post-growth thermal annealing^{17–19} (see the Methods section). The absorption spectra of the annealed samples with temperatures ranging from 800 to 900 °C are shown in Fig. 1c (the absorption spectrum for the quantum-dot sample annealed at 800 °C is not

shown because it overlaps strongly with the Reststrahlen band). The absorption spectra show several interesting features: (1) the absorption of annealed-sample peaks below the Reststrahlen band, with increasing redshift for increasing annealing temperature; (2) the material interdiffusion induced by the annealing does not eliminate the anisotropic splitting, which diminishes only slightly to about 2 meV; and (3) the lines become broader, indicating an enhancement of size and composition inhomogeneity of the dots during the annealing. These results clearly demonstrate that post-growth annealing provides a well-controlled means to obtain dots with average intersublevel spacing Δ_{sp} well below the Reststrahlen band (for example, $\Delta_{sp} \sim 10$ meV (2.4 THz) for the 900 °C sample).

The relaxation dynamics of excited carriers in quantum dots are studied using degenerate terahertz pump-probe spectroscopy. A free-electron laser ‘FELBE’ delivering linearly polarized picosecond pulses was used in the experiments²⁰. An initial pulse excites the ground state to the p_x or p_y transition (the in-plane light polarization is chosen parallel to either of the crystallographic axes), and a second pulse probes the recovery of the absorption signal for this same transition as a function of the time delay between the pump and probe pulses. The results of low-temperature (10 K) pump-probe measurements for different excitation energies are shown in Fig. 2a. We observe a very strong variation in the recovery of the absorption bleaching when changing the transition energy. For transition energies close to the longitudinal optical

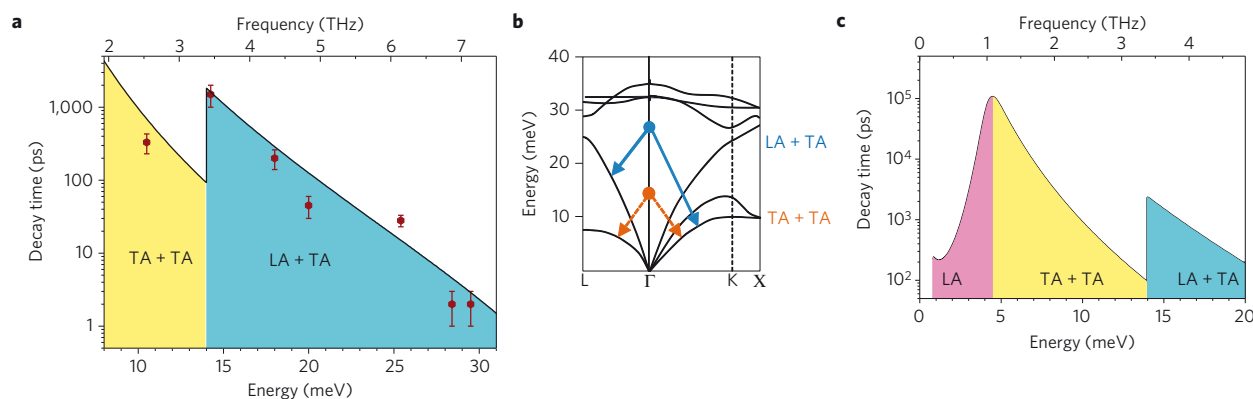


Figure 3 | Intersublevel lifetimes in the terahertz region. **a**, Variation of the decay time with the transition energy below the Reststrahlen band: experimental data (symbols) and theoretical calculations (solid line). The error bars are determined by the uncertainty in the mono-exponential decay fit. **b**, Schematic diagram of the different polaronic decay channels. **c**, Calculation of the relaxation time in an $\text{In}_{0.1}\text{Ga}_{0.9}\text{As}/\text{GaAs}$ quantum dot of varying diameter showing the transition between electron relaxation by emission of one acoustic phonon (below ~ 1 THz) and the polaron anharmonic decay (above ~ 1 THz).

phonon energy, the decay curve is mono-exponential with a short time constant varying from 2 ± 1 ps for ~ 30 meV (≈ 7.2 THz) up to 60 ± 5 ps for 20 meV (≈ 4.8 THz). With a further decrease of the transition energy, the time dynamic presents a bi-exponential decay. The mono-exponential decay time as well as the extracted long time component in the bi-exponential case is plotted as a function of the transition energy in Fig. 3a. The decay time increases strongly with decreasing transition energy up to 1.5 ± 0.5 ns at ~ 15 meV (≈ 3.6 THz).

We assign the mono-exponential decay as well as the long time component in the bi-exponential case to the decay from the p to the s shells of the quantum-dot levels, whereas the short time component results from population interchanges among the p states (p_x and p_y) by absorption or emission of acoustic phonons with energy corresponding to the anisotropic splitting $\Delta_{pp} \approx 2$ meV (see Fig. 2b). This interpretation is corroborated by further measurements in the bi-exponential regime, using light with opposite in-plane polarization to probe also the p_y transition (see Fig. 2c). The initial decay is faster when exciting an upper (p_y) state than a lower (p_x) one, as expected because at low temperature, phonon emission is much more probable than absorption. This interpretation is confirmed in Fig. 2d when comparing the experimental data to simulations (dashed lines) that include the calculated rates for the thermal exchange between the p_x and p_y levels. This model also provides a clear explanation for the absence of bi-exponential behaviour for energies above ~ 20 meV, because the p_x to s relaxation time is shorter than or comparable to the $p_x - p_y$ thermalization time.

Let us focus now on the interpretation of the strong energy dependence of the p -to- s intersublevel relaxation time, reported in Fig. 3a as a function of the intersublevel detuning. We expect that the scattering mechanisms responsible for the energy relaxation in bulk and quantum wells are either forbidden (elastic) or greatly reduced (inelastic) in quantum dots, owing to the discrete nature of the energy levels^{21,22}. Instead, as we show below, the anharmonic decay of quantum-dot polarons (electrons strongly coupled to longitudinal optical phonons^{23–25}) is the dominant relaxation mechanism below the longitudinal optical phonon energy down to the 1 THz regime. This is the same physical mechanism that has been shown previously to lead to efficient relaxation at energies above the longitudinal optical phonon energy^{9–13} (between 20 and 65 ps in the 40–60 meV energy range¹⁰), but producing here a much higher sensitivity of the cooling rate with the amount of relaxed energy. This demonstrates the generality of the polaron formation and decay mechanism for energy relaxation in systems with

three-dimensional quantization of the electronic states. We have calculated the intersublevel relaxation time using the microscopic model of anharmonic polaron decay developed in ref. 13 (see the Methods section). The Fröhlich polar coupling between electrons and longitudinal optical phonons is taken into account and leads to the formation of polaron states. The anharmonic terms of the lattice vibrational potential energy then trigger the polaron disintegration into a two-phonon state. We incorporate the three possible channels for two-phonon disintegration allowed in the studied energy range: LA + LA, LA + TA and TA + TA, where LA corresponds to longitudinal acoustic and TA to transverse acoustic phonons, as shown schematically in Fig. 3b. The calculated lifetime is plotted in Fig. 3a as a function of the transition energy. For each decay channel, the relaxation rate strongly decreases with decreasing intersublevel energy. Three factors mainly contribute to this behaviour: the reduction of the available density of two-acoustic-phonon states, the decreasing strength of the anharmonic couplings involved and the increasing detuning with respect to the longitudinal optical phonon energy. We find that the LA + TA channel dominates for intersublevel energies below ~ 33 meV (8 THz) (the longitudinal acoustic Debye energy plus the transverse acoustic Debye energy) but larger than twice the transverse acoustic Debye energy (taken as 7 meV here). Below ~ 14 meV, the TA + TA path becomes available, which explains the non-monotonic variation in the calculated and measured times around this energy.

In addition, we carried out pump-probe measurements at a temperature higher than 10 K at energies of 25.4 meV and 14.25 meV (see Supplementary Information). At transition energies around 25.4 meV, the temperature dependence of the intersublevel lifetime, which decreases from 28 ± 2 ps at 10 K to 8 ± 3 ps at 170 K, can be well fitted considering polaron decay into two acoustic phonons (TA + LA). For a pump-probe energy of 14.25 meV, the intersublevel lifetime was measured to decrease from 1.5 ± 0.5 ns at 10 K to 560 ± 50 ps at 30 K and 260 ± 30 ps at 50 K. At this energy, a polaron decay time of 60 ps is expected at room temperature.

The overall close agreement between experiment and theory demonstrates that the energy relaxation in annealed SAQDs is governed by the anharmonic mechanism and becomes strongly inhibited when the level spacing decreases to the order of a few terahertz. However, it is known that in lithographically defined quantum dots, where the s - p transition energy is below 1 THz, an efficient cooling of carriers is ensured by the emission of one acoustic phonon^{26,27}. To show the crossover between the two regimes, we have calculated the intersublevel lifetime for

transition energies between 1 and 5 meV in quantum dots with fixed composition ($\text{In}_{0.1}\text{Ga}_{0.9}\text{As}/\text{GaAs}$) and fixed height (5 nm) and varying diameter. As shown in Fig. 3c, one-phonon emission does provide an efficient relaxation channel in the sub-terahertz domain, but quickly becomes inoperative for larger intersublevel energies. As a consequence of this acoustic-phonon bottleneck, the anharmonic polaron decay mechanism governs the p -to- s energy relaxation in SAQDs down to the 1 THz regime.

Our studies demonstrate that carrier cooling in quantum dots in the terahertz domain is due to the mechanism of anharmonic polaron decay, and that its rate increases by about three orders of magnitude when the energy spacing varies between 7 and 3.5 THz. This extreme sensitivity is a consequence of the polaronic nature of the relaxation processes in fully confined quantum dots. Our results provide important new information for the design of quantum-dot-based terahertz optoelectronic devices. The long carrier relaxation times, and the ability to controllably alter the times by varying the sublevel spacing, provide strong motivation for the production of, for example, terahertz lasers, which require the inhibition of the upper-to-lower relaxation and a fast emptying of the lower level.

Methods

Annealing. The annealing was carried out in a rapid thermal annealer with temperatures ranging from 800 to 900 °C. The annealing time was fixed to 4 min. During the annealing process, the samples were sandwiched between two GaAs wafers to prevent As out-diffusion from the sample surface and were kept in a nitrogen ambient environment. We prepared several samples annealed at 800, 820, 850, 875 and 900 °C to cover the investigated spectral range.

Experimental set-up. The degenerate terahertz pump-probe measurements were carried out using the Free Electron Laser Facilities 'FELBE' located at Forschungszentrum Dresden-Rossendorf (Germany)²⁰. The free-electron laser delivered linearly polarized picosecond pulses with a repetition rate of 13 MHz tunable in the 18–250 μm spectral range. The laser beam was split into pump and probe beams with pulse energies of ~ 1 and ~ 0.01 nJ correspondingly. The pump beam was modulated at a frequency of ~ 330 Hz using an optical chopper and a variable time delay between the pump and probe was introduced. An off-axis parabolic mirror of ~ 11 cm effective focal length was applied to focus both the pump and the probe beam onto the same spot on the sample, which was held in a He-flow cryostat with diamond windows. The pump and probe beams were hitting the sample at about a 10° angle to the normal. The change of the intensity of the probe beam after the sample was detected using a Ge:Ga detector and a lock-in amplifier, which was locked to the modulation frequency of the pump beam. Owing to the high repetition rate and stability of the laser, we were able to resolve an absorption change as small as $\sim 0.05\%$. A mirror-based polarization rotator was also incorporated into the incident beam path to enable us to pump and probe either s - p_x or s - p_y quantum-dot transitions.

Modelling of the interdiffused quantum dots. We model both as-grown and annealed $\text{In}_x\text{Ga}_{1-x}\text{As}/\text{GaAs}$ dots as truncated cones with in-plane (top) basis radius R ($R/2$), height h and uniform In fraction x in the dot region, residing on a thin wetting layer of the same In concentration, and surrounded by GaAs. The parameters of the as-grown quantum dots ($R_0 = 122$ Å, $h_0 = 49$ Å, $x_0 = 0.55$) were chosen to fit both intersublevel and interband transition energies ($\Delta_{\text{sp}} \approx 48$ meV and the photoluminescence peak is centred at 1,109 meV). For annealed dots, we assume that: (1) the In quantity inside the dot and the aspect ratio R/h are both preserved during the thermal process, which gives $R = R_0(x_0/x)^{1/3}$ for the annealed dot; (2) the confining potential depth ΔV varies linearly with the In content: $x_0 \Delta V = x \Delta V_0$. Despite its simplicity, this model captures the main aspects of the interdiffusion, namely, an increase of the quantum-dot effective size and a decrease of its confinement potential, which both lead to a decrease of Δ_{sp} . We calculate that Δ_{sp} decreases from 48 to 10 meV on increasing the quantum-dot radius from $R \sim 12$ to ~ 25 nm with a corresponding decrease of the In fraction from $x \sim 0.55$ to 0.07. The corresponding electron wavefunctions are used to calculate the matrix elements related to the coupling of the confined electron to both the acoustical and optical phonons. In particular, the Fröhlich coupling V_{sp} (see ref. 13 for definition) varies from 3.2 meV for $\Delta_{\text{sp}} = 30$ to 2.5 meV when $\Delta_{\text{sp}} = 10$ meV.

Anharmonic decay of polarons. The intersublevel relaxation time is calculated using the microscopic model in ref. 13. We use channel-dependent Gruneisen constants to fit the present data: $\gamma = 1.3$ for the LA + LA channel (as in ref. 13), and $\gamma = 4.0$ for the TA + TA and TA + LA channels. The transverse acoustic and longitudinal acoustic Debye energies are taken respectively as 7 and 26 meV. In the present work, we take into account the non-resonant Fröhlich couplings between

the ground state and the longitudinal optical phonon replicas of the p states. As a consequence, we find that the polaron decay time τ due to the anharmonic couplings is given by:

$$\frac{\hbar}{\tau} = \frac{4\Delta_{\text{sp}}^2}{(\hbar\omega_{\text{LO}} + \Delta_{\text{sp}})^2} \frac{V_{\text{sp}}^2}{(\Delta_{\text{sp}} - \hbar\omega_{\text{LO}})^2 + V_{\text{sp}}^2} \Gamma^{\text{ph}}(\Delta_{\text{sp}}) \quad (1)$$

where the function $\Gamma^{\text{ph}}(E)$ is defined in ref. 13. The intersublevel transition energy Δ_{sp} corresponds to the optically probed transition energy between s -like and p -like polaron states with a dominant zero-phonon component. This formula is used here instead of formula (6) used in ref. 13, which is valid only close to the longitudinal optical phonon resonance. The first term in the above equation arises from the interference between the resonant and the non-resonant couplings. This interference is found to be destructive for intersublevel transition energies that are small compared with the longitudinal optical phonon one ($\Delta_{\text{sp}} \ll \hbar\omega_{\text{LO}}$). This effect contributes also to the inhibition of the polaron decay mechanism at low energies, in particular in the calculation shown in Fig. 3c.

Received 15 April 2009; accepted 14 July 2009; published online 16 August 2009

References

1. Faist, J. *et al.* Quantum cascade laser. *Science* **264**, 553–556 (1994).
2. Kohler, R. *et al.* Terahertz semiconductor-heterostructure laser. *Nature* **417**, 156–159 (2002).
3. Urayama, J., Norris, T. B., Singh, J. & Bhattacharya, P. Observation of phonon bottleneck in quantum dot electronic relaxation. *Phys. Rev. Lett.* **86**, 4930–4933 (2001).
4. Borri, P. & Langbein, W. Four-wave mixing dynamics of excitons in InGaAs self-assembled quantum dots. *J. Phys. Condens. Matter* **19**, 295201 (2007).
5. Botez, D. *et al.* Progress towards intersubband quantum-box lasers for highly efficient continuous wave operation in the mid-infrared. *J. Nanophoton.* **3**, 031606 (2009).
6. Murdin, B. N. *et al.* Direct observation of the LO phonon bottleneck in wide GaAs/Al_xGa_{1-x}As quantum wells. *Phys. Rev. B* **55**, 5171–5176 (1997).
7. Hartig, M. *et al.* Efficient intersubband scattering via carrier-carrier interaction in quantum wells. *Phys. Rev. Lett.* **80**, 1940–1943 (1998).
8. Wade, A. *et al.* Magnetic-field-assisted terahertz quantum cascade laser operating up to 225 K. *Nature Photon.* **3**, 41–45 (2008).
9. Sauvage, S. *et al.* Long polaron lifetime in InAs/GaAs self-assembled quantum dots. *Phys. Rev. Lett.* **88**, 177402 (2002).
10. Zibik, E. A. *et al.* Intraband relaxation via polaron decay in InAs self-assembled quantum dots. *Phys. Rev. B* **70**, 161305(R) (2004).
11. Li, X.-Q., Nakayama, H. & Arakawa, Y. Phonon bottleneck in quantum dots: Role of lifetime of the confined optical phonons. *Phys. Rev. B* **59**, 5069–5073 (1999).
12. Verzele, O., Ferreira, R. & Bastard, G. Polaron lifetime and energy relaxation in semiconductor quantum dots. *Phys. Rev. B* **62**, 4809–4812(R) (2000).
13. Grange, T., Ferreira, R. & Bastard, G. Polaron relaxation in self-assembled quantum dots: Breakdown of the semiclassical model. *Phys. Rev. B* **76**, 241304(R) (2007).
14. Nabetani, Y. *et al.* Initial growth stage and optical properties of a three-dimensional InAs structure on GaAs. *J. Appl. Phys.* **76**, 347–351 (1994).
15. Stier, O. *et al.* Electronic and optical properties of strained quantum dots modeled by 8-band k.p theory. *Phys. Rev. B* **59**, 5688–5701 (1999).
16. Bester, G. *et al.* Pseudopotential calculation of the excitonic fine structure of million-atom self-assembled $\text{In}_{1-x}\text{Ga}_x\text{As}/\text{GaAs}$ quantum dots. *Phys. Rev. B* **67**, 161306 (2003).
17. Fafard, S. *et al.* Manipulating the energy levels of semiconductor quantum dots. *Phys. Rev. B* **59**, 15368–15373 (1999).
18. Fafard, S. & Allen, C. Ni. Intermixing in quantum-dot ensembles with sharp adjustable shells. *Appl. Phys. Lett.* **75**, 2374–2376 (1999).
19. Zibik, E. A. *et al.* Effects of alloy intermixing on the lateral confinement potential in InAs/GaAs self-assembled quantum dots probed by intersublevel absorption spectroscopy. *Appl. Phys. Lett.* **90**, 163107 (2007).
20. Lehnert, U. *et al.* Proc. 29th FEL Conference, Novosibirsk, Russia (2007); available at <<http://accelconf.web.cern.ch/AccelConf/f07/PAPERS/MOPPH036.PDF>>.
21. Bockelman, U. & Bastard, G. Phonon scattering and energy relaxation in two-, one-, and zero-dimensional electron gases. *Phys. Rev. B* **42**, 8947–8951 (1990).
22. Benisty, H., Sotomayor-Torres, C. M. & Weisbuch, C. Intrinsic mechanism for the poor luminescence properties of quantum-box systems. *Phys. Rev. B* **44**, 10945–10948 (1991).
23. Inoshita, T. & Sakaki, H. Density of states and phonon-induced relaxation of electrons in semiconductor quantum dots. *Phys. Rev. B* **56**, R4355–R4358 (1997).

24. Hameau, S. *et al.* Strong electron–phonon coupling regime in quantum dots: Evidence for everlasting resonant polarons. *Phys. Rev. Lett.* **83**, 4152–4155 (1999).
25. Carpenter, B. A. *et al.* Intraband magnetospectroscopy of singly and doubly charged *n*-type self-assembled quantum dots. *Phys. Rev. B* **74**, 161302(R) (2006).
26. Garcia, C. P. *et al.* Evidence of correlation in spin excitations of few-electron quantum dots. *Phys. Rev. Lett.* **95**, 266806 (2005).
27. Fujisawa, T. *et al.* Allowed and forbidden transitions in artificial hydrogen and helium atoms. *Nature* **419**, 278–281 (2002).

Acknowledgements

Financial support was provided by the UK Engineering and Physical Sciences Research Council (EPSRC). The LPA (UMR 8551) is associated with the CNRS and the Universities Paris 6 and Paris 7. The free-electron laser 'FELBE' is supported by the Integrating Activity on Synchrotron and Free-Electron Laser Science (IA-SFS) under the EU contract RII3-CT-2004-506008 of the 6th Framework 'Structuring the European Research Area,

Research Infrastructures Action'. We are grateful to P. Michel and the FELBE team for their dedicated support.

Author contributions

E.A.Z. and L.R.W. conceived the experiments; E.A.Z., L.R.W., B.A.C., N.E.P., D.S. and S.W. carried out the experiments; T.G., R.F. and G.B. made the theory and modelled the experiments; E.A.Z. and T.G. analysed the data; L.R.W., R.F., E.A.Z. and M.S.S. supervised the project; H.Y.L. grew the samples; T.G., E.A.Z., R.F. and L.R.W. wrote the paper with major input and edits from M.S.S. and M.H. All authors discussed the results and commented on the manuscript.

Additional information

Supplementary information accompanies this paper on www.nature.com/naturematerials. Reprints and permissions information is available online at <http://npg.nature.com/reprintsandpermissions>. Correspondence and requests for materials should be addressed to R.F. or L.R.W.